

PAPER

A Robust Approach for Ulcer Classification/Detection in WCE Images

Abdellatif Dahmouni¹(✉),
Abdelkafer Ait
Abdelouahad¹, Yasser
Aderghal¹, Ibrahim Guelzim²,
Insaf Bellamine¹, Hassan
Silkan¹

¹LAROSERI Faculty of Sciences,
Chouaib Doukkali University,
El Jadida, Morocco

²Computer Engineering ISPS2I
NSAC, Hassan 2 University,
Casablanca, Morocco

dahmouni.a@ucd.ac.ma

ABSTRACT

Wireless Capsule Endoscopy (WCE) is a medical diagnostic technique recognized for its minimally invasive and painless nature for the patients. It uses remote imaging techniques to explore various segments of the gastrointestinal (GI) tract, particularly the hard-to-reach small intestine, making it an effective alternative to traditional endoscopic techniques. However, physicians face a significant challenge when it comes to analyzing a large number of endoscopic images due to the effort and time required. It is therefore imperative to implement aided-diagnostic systems capable of automatically detecting suspicious areas for subsequent medical assessment. In this paper, we present a novel approach to identify gastrointestinal tract abnormalities from WCE images, with a particular focus on ulcerated areas. Our approach involves the use of the Median Robust Extended Local Binary Pattern (MRELBP) descriptor, which effectively overcomes the challenges faced when WCE image acquisition, such as variations in illumination and contrast, rotation, and noise. Using machine learning algorithms, we conducted experiments on the extensive Kvasir-Capsule dataset, and subsequently compared our results with recent relevant studies. Noteworthy is the fact that our approach achieved an accuracy of 97.04% with the SVM (RBF) classifier and 96.77% with the RF classifier.

KEYWORDS

WCE, computer-aided-diagnostic, machine learning, deep learning, Completed LBP, Median Robust Extended LBP

1 INTRODUCTION

Medical imaging is an essential tool that allows physicians to accurately diagnose patients without resorting to invasive processes, by providing a preliminary view of the condition of the human body. In order to precisely detect various abnormalities, physicians currently undertake the difficult task of manually examining an extensive collection of medical images for each assessment. This process

Dahmouni, A., Abdelouahad, A.A., Aderghal, Y., Guelzim, I., Bellamine, I., Silkan, H. (2024). A Robust Approach for Ulcer Classification/Detection in WCE Images. *International Journal of Online and Biomedical Engineering (iJOE)*, 20(6), pp. 86–102. <https://doi.org/10.3991/ijoe.v20i06.45773>

Article submitted 2023-10-10. Revision uploaded 2023-12-08. Final acceptance 2023-12-08.

© 2024 by the authors of this article. Published under CC-BY.

requires more effort and time, contributing to the exhaustion and monotony of the screening process. Contemporary scientific research has focused on the development of computer systems with the ability to autonomously analyze and interpret big medical images data [1, 2, 3]. These systems must cover all medical images acquisition modalities, such as X-rays, mammography, ultrasound, tomography, magnetic resonance imaging, cardiography and endoscopy. Gastrointestinal diseases are among the most common and difficult to diagnose illnesses [4]. Recently, gastrointestinal endoscopy has advanced significantly, with the emergence of various endoscopic types, including colonoscopy [5], gastroscopy [6], narrow-band imaging endoscopy [7], zoom-endoscopy [8], and the more recent wireless capsule endoscopy (WCE) [9]. In fact, the wireless capsule has completely revolutionized the endoscopy field by effectively supplanting the conventional endoscopic tubes. This pill-shaped image capture apparatus enables for a perfectly non-invasive visualization of the gastrointestinal tract. During the WCE endoscopy process, a patient consumes the pill-shaped device containing a camera that travels through the gastrointestinal tract, capturing and transmitting images to an external receiver. These high-resolution (RGB) images are recorded as a video comprising over 60,000 images per examination and patient [10]. The in-depth analysis of all these images should be done by expert physicians. In addition, identifying, localizing, and treating affected areas becomes extremely difficult, especially since only 5% of these images typically depict abnormalities [11]. Hence the need for computer-aided techniques for efficient and autonomous processing of WCE images to determine the size and location of various lesions in the gastrointestinal tract, including tumors [12], ulcers [13], polyps [14] and bleeding [15].

Several studies have been conducted to investigate gastrointestinal tract using endoscopic images. The majority of them have been focused on the analysis of WCE images' textural features. We can distinguish two main approaches: machine learning-based methods and deep learning-based methods. The first approach involves a series of steps, namely preprocessing, features extraction and careful selection, learning and classification. In the second approach, the previous steps are combined into the same CNN-architecture to process feature sets for specific problems. In this paper, we propose a novel approach for automatic ulcer disease processing in WCE images, which mainly aims to solve problems related to shooting conditions, such as variations in illumination and contrast, rotation, and noise. In this approach, we use the Power Law Transformation (PLT) algorithm to enhance the contrast of RGB and YCbCr images. These enhanced images are then used to extract specific ulcer features using the MRELBP descriptor [16]. The Spatially Enhanced Local Binary Pattern Histogram (eLBPH) [17] was used to build the final feature vector. Finally, we classify feature dataset using machine learning algorithms, including Support Vector Machines (SVMs), Random Forest (RF), Multilayers Perceptron (MLP) and K-Nearest Neighbor (KNN). By adopting this strategy, we succeed in improving the results of state-of-the-art machine learning-based methods as well as demonstrating the competitiveness of the proposed approach compared to some of deep learning-based methods. The remainder of this paper is organized as follows: In Section 2, the related work is presented. Section 3 is reserved for a detailed description of the proposed approach. Experimental results and discussion are presented in Section 4. Finally, the paper ends with conclusion.

2 RELATED WORK

Ulcer is an open lesion in the mucous membrane of the stomach or intestine. Peptic ulcers can manifest themselves as pain, digestive bleeding or even perforation, and when it is chronic, peptic ulcers can degenerate into cancer [18, 19]. Thus, an early treatment of ulcers can prevent cancer. Moreover, some cancers can take on an ulcerated form and be mistaken for ulcers. Fortunately, artificial intelligence has now given rise to computer-assisted diagnosis. These systems, based on image processing algorithms and computer vision techniques, make it possible to visualize the entire digestive tract and detect its abnormalities. This means that more patients can be examined than ever before. This paper focuses on the detection of ulcers as one of the common gastrointestinal (GI) pathologies. In this section, we present a state-of-the-art review of the most recent and relevant methods for ulcer detection in endoscopic video capsule images. For this purpose, we will divide these methods into two families: deep learning-based methods and machine learning-based methods.

2.1 Deep learning-based methods

Deep learning techniques have been widely applied across various research domains. These techniques are divided into two categories: the Layers-CNN-model, tailored to specific requirements, and the pre-trained-CNN-model. Which leverages learning transfer using established frameworks like ResNet, VGGNet, GoogleNet, VGG-16, and AlexNet [20, 21]. Consistently, Lakovidis et al. implemented a two-step approach comprising a Deep Saliency Detection (DSD) algorithm for salient points detection and a Weakly Supervised Convolutional Neural Network (WCNN) for classification [22]. In fact, DSD makes it possible to locate data key characteristics in order to better understand the underlying structures. Additionally, WCNN uses partial information to infer desired patterns within selected salient regions. Tomonori et al. [23] proposed an automatic detection of ulcerations in WCE images based on a deep convolutional neural network. The architecture involved is named Single Shot Multi-Box Detector (SSD) and was introduced a few years before by Wei Liu et al. [24]. The defining feature of this architectural framework is its ability to generate a diverse set of bounding boxes at various scales, enabling simultaneous object detection and localization. The results were promising and encouraging, since the accuracy achieved 90%. In their paper [25], Sen Wang et al. wanted to find out how well deep learning would work for ulcer detection. To this end, they proceeded in two phases. First, they started by understanding the task of ulcer detection, and the basics behind classic deep learning networks. Second, they proposed a new architecture named HANet and based on the ResNet-34, a CNN known for its depth and its ability to alleviate the challenges associated with training extremely deep networks. Haya Alaskar et al. [26] proposed an analysis of two distinct CNN architectures, namely AlexNet [27] and Google-Net [28]. They aim to study their ability to distinguish between ulcer and non-ulcer WCE images. They also provide a comparison with some relevant machine learning-based approaches. Indeed, this contribution marks the beginning of scientific discourse concerning the utilization of deep learning in the analysis of medical images, particularly in the assessment of WCE-based gastrointestinal pathology. Vani et al. [29] introduced a four-layered deep learning Convolutional Neural Network (CNN) for the detection of ulcers in

WCE images. Furthermore, the proposed model highlights a hierarchical feature extraction process inherent to deep neural networks. Concurrently, Rehman [30] proposed a two-step process for identifying ulcers. First, a Region of Interest (ROI) is implemented to detect suspicious areas based on a thresholding. Then, these ROIs feed a 6-layers convolutional neural network model. Both contributions underscore the exploration of deep learning-based methodology for improved ulcer detection efficiency in WCE images. Ellahyani et al. [31] used fine-tuned convolutional neural networks to extract relevant features from WCE images. The Random Forest classifier was then employed to identify ulcerous images based on the extracted features. This approach validates the efficacy of feature extraction by amalgamating the decision-making capabilities of both machine learning and deep learning techniques. In [32], a pre-processing step was made to increase the quality of the input images for classification. This pre-processing consists of achieving contrast and illumination invariance, aiming to normalize and optimize the quality of the input image for subsequent analysis. The fused image dataset then represents the input of a deep learning model named Mobil-Netv2. Certainly, Mobilnetv2 is an efficient CNN architecture, particularly suitable for resource-constrained applications, like ulcer classification in WCE images.

2.2 Machine learning-based methods

A number of studies focusing on the automatic detection of ulcers have been conducted using machine learning techniques. For example, Baopu et al. [33] introduced a new scheme based on the curvelet transform and the LBP for a robust feature description. This scheme was combined with machine learning methods such as Multilayer Perceptron (MLP) and Support Vector Machines (SVM). In [34], the Bidimensional Ensemble Empirical Mode Decomposition (BEEMD) was employed to extract different intrinsic mode functions. In addition, a lacunarity method was involved to capture the fractal property of WCE images. Finally, a simple discriminant analysis-based classification served as a classifier. This approach holds significant implications for the analysis of medical images and the classification of gastrointestinal pathologies. Lecheng et al. [35] investigated the use of the bag-of-words model after its success in several computer vision algorithms. Two texture descriptors were involved to describe WCE images, namely LBP and SIFT. The SVM algorithms were used as classifiers. Jinn-Yi et al. [36] proposed the use of color features to categorize WCE images into normal, bleeding or ulcerous ones, mainly, descriptors of color coherence vectors and gray level co-occurrence matrices. In addition, spatial and statistical features like contrast, energy, correlation and homogeneity, were then computed. Finally, several classifiers were involved such as SVM, decision tree, neural networks and others. The results of this study guided the choice of methods according to the specificities of the medical data and classification needs. Charfi et al. [37] proposed a methodology that involves segmenting WCE images using saliency and color maps, extracting features using Color LBP (CLBP) and Pyramid Orientation Histograms (PHOG), and classifying features data using SVM, MLP, and HMM. Furthermore, Souaidi et al. [38] proposed to capture supplementary texture information with the (MS-CLBP) descriptor and both YCbCr and RGB color spaces. The SVM algorithms were employed as classifiers. Therefore, this comparative study provided valuable insights into the choosing suitable descriptors and classifiers, contributing to the effective analysis of WCE images. Ponnusamy et al. [39] proposed a fusion of texture and color features by the use

of center symmetric local binary pattern (CS-LBP), scale invariant feature transform (SIFT) and the auto color correlogram (ACC). Similarly, to the bag-of-words, this combination leads to a visual bag of features that can be employed to identify the status of the gastrointestinal tract. Also, for the classification, they used SVM. This study provided crucial insights that can be taken into account when using the CS-LBP, SIFT, and ACC appearance descriptors in medical imaging. A small number of authors have proposed a hybrid approach making use of both deep learning and machine learning techniques. For example, Naz et al. [40] proposed a method in which they used filtering techniques to enhance the contrast of WCE images. Then, they performed feature extraction using a hybrid method consisting of LBP, SFTA, VGG16 and InceptionV3. Finally, SVMs, KNN, MLP, B-Trees and RF are used as classifiers.

3 MOTIVATION AND METHODOLOGY

In this section, the proposed approach for identifying ulcer abnormalities in WCE images is presented.

3.1 Proposed scheme

As shown in Figure 1, our proposed system consists of four stages: pre-processing, features extraction, statistical features selection and classification. In the pre-processing stage, the contrast of input WCE images is enhanced using the PLT algorithm [41], then decomposed into a specific's components (C1, C2 and C3) of each color space (RGB or YCbCr). The second stage involves the MRELBP descriptor to more discriminate ulcer-prone areas within each color component. In the third stage, eLBPH is used to build the final features vectors as histograms. Finally, the SVMs, RF, MLP and KNN classifiers occur at the last stage.

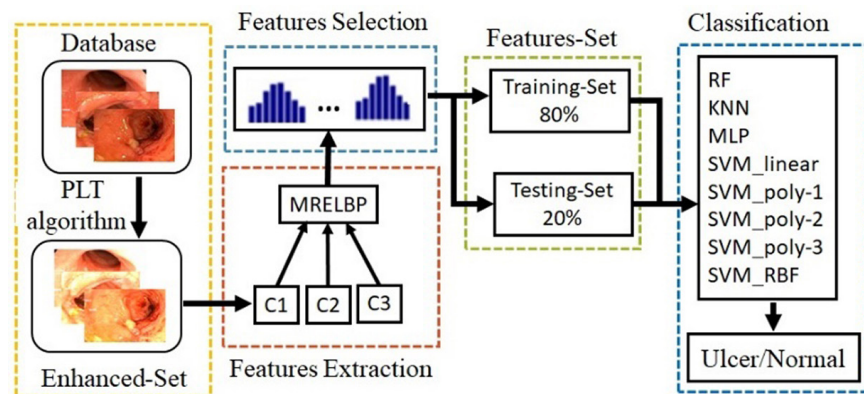


Fig. 1. The aided-diagnostic system proposed scheme

3.2 Pre-processing

Generally, WCE images are low quality (contrast and color), they do not allow accurate detection of abnormal areas. In order to improve the quality of WCE images, we applied two steps. In the first, we improve contrast by using (PLT) algorithm

usually defined as: $\alpha = C \times P\beta$, where, α is the value transformed pixel; P is the value of the original pixel; and C and β are constants that need to be well chosen to get the best transformation. In our case, we take the same values from [32], i.e., $C = 1.5$ and $\beta = 0.9$. In the second, we try to determine precisely which components of the RGB (R, G or B) and YCbCr (Y, Cb or Cr) color spaces are most suitable for our system.

3.3 Features extraction and selection

During many image-based pattern recognition studies, LBP-like methods have been verified as effective feature extractors. In our case, we use two variants: 1) CLBP which detects the magnitude of the light spots on the edge. And 2) MRELBP is widely renowned for its robustness to noise and its scale invariance.

Brief review of LBP. Local Binary Patterns (*LBP*) is one of the popular texture operators initially proposed by Ojala [42] and extended to several pattern recognition applications. *LBP* is computed for the current pixel by comparing its grayscale value with the values of its immediate neighbors. This process can be expressed as follows:

$$LBP_{P,R}(x_c) = \sum_{p=0}^{P-1} S(x_p - x_c)2^p. \text{ Where, } S(x) = \begin{cases} 1 & \text{if } x \geq 0 \\ 0 & \text{if } x < 0 \end{cases} \quad (1)$$

Where x_c and x_p denote the current and neighboring pixels, P is the total number of neighboring pixels, R is the radius of the neighborhood and $S(\cdot)$ is the sign function.

To address some *LBP* shortages, many *LBP* variants are proposed, mainly the Rotation Invariant Uniform *LBP* (LBP^{riu2}), which improves robustness against image rotations and reduces histogram range values [43].

Brief review of Completed LBP (CLBP). *CLBP* [44] is an extension of *LBP* that describes the local area of image by the Local Difference Sign-Magnitude Transform (LDSMT). Which consists of two components: the sign component (*CLBP_S*) and the magnitude component (*CLBP_M*). Given a current pixel x_c with P neighboring pixels x_p , the LDSMT between x_c and x_p is denoted d_p . To compute *CLBP_S* and *CLBP_M*, d_p is decomposed into the sign component s_p and magnitude component m_p as (Eq.2).

$$d_p = x_p - x_c = s_p \times m_p. \text{ Where } s_p = \text{sign}(d_p) \text{ and } m_p = |x_p - x_c| \quad (2)$$

Then, s_p is used to compute *CLBP_S* as (Eq.3).

$$CLBP - S_{P,R}(x_c) = \sum_{p=0}^{P-1} t(x_p - x_c)2^p. \text{ Where, } t(x) = \begin{cases} 1 & \text{if } x \geq 0 \\ 0 & \text{if } x < 0 \end{cases} \quad (3)$$

whereas, m_p is used to build *CLBP_M* as (Eq.4).

$$CLBP - M_{P,R}(x_c) = \sum_{p=0}^{P-1} t(m_p, c)2^p. \text{ Where, } t(x, c) = \begin{cases} 1 & \text{if } x \geq c \\ 0 & \text{if } x < c \end{cases} \quad (4)$$

And c is an adaptive threshold

Moreover, current pixel x_p is used to define a new operator, called CLBP-Center (*CLBP_C*) as (Eq.5).

$$CLBP - C_{p,R}(x_c) = t(x_c, c_0). \text{ Where, } t(x, c_0) = \begin{cases} 1 & \text{if } x \geq c_0 \\ 0 & \text{if } x < c_0 \end{cases} \quad (5)$$

Where, c_0 is the average gray level of the whole image

Finally, $CLBP_S$, $CLBP_M$ and $CLBP_C$ are combined together to construct the $CLBP$ histogram features.

Brief review of Median robust extended LBP (MRELBP). MRELBP is an enhanced extension of LBP initially introduced by Liu et al. [16] to address some of the LBP limitations, such as multiresolution problem, noise sensitivity and rotation variation. As a new texture descriptor, MRELBP describes each current pixel using the three variants of $RELBP$ descriptor [45], namely, central intensity pixel description ($RELBP_{CI}$), neighborhood intensity pixel description ($RELBP_{NI}$) and radial difference pixel description $RELBP_{RD}$. Given a current pixel x_c , $RELBP_{CI}$, $RELBP_{NI}$, and $RELBP_{RD}$ are defined as follows:

- Central intensity representation (Eq.6).

$$RELBP_{CI}(x_c) = S(\phi(X_{c,w}) - \mu_w) \quad (6)$$

In this formula, $S(.)$ is the sign function, $\phi(.)$ is the filter of size $w \times w$, $X_{c,w}$ is the local patch centered on pixel x_c and μ_w is the average of $\phi(X_{c,w})$ over the whole image.

- Neighborhood intensity representation (Eq.7).

$$RELBP_{NI}_{r,p}(x_c) = \sum_{n=0}^{p-1} S\left(\phi\left(X_{r,p,w_r,n}\right) - \mu_{r,p,w_r}\right) 2^n \quad (7)$$

$$\text{Where, } \mu_{r,p,w_r} = \frac{1}{p} \sum_{n=0}^{p-1} \phi\left(X_{r,p,w_r,n}\right)$$

In this formula, $X_{r,p,w_r,n}$ denotes a patch of size $w_r * w_r$ centered on $x_{r,p,n}$.

- Radial difference representation (Eq.8).

$$RELBP_{RD}_{r,r-1,p,w_r,w_{r-1}}(x_c) = \sum_{n=0}^{p-1} S\left(\phi\left(X_{r,p,w_r,n}\right) - \phi\left(X_{r-1,p,w_{r-1},n}\right)\right) 2^n \quad (8)$$

Where, $X_{r,p,w_r,n}$ and $X_{r-1,p,w_{r-1},n}$ denote patches centered on $x_{r,p,n}$ and $x_{r-1,p,n}$ neighboring pixels, respectively.

Features histograms extraction. In the original eLBPH, the texture image is first divided into d regions R_0, \dots, R_{d-1} , reduced LBP^{u2} histograms of these regions are separately computed and then concatenated into a single histogram that represents the eLBPH feature vector. In addition, the same eLBPH principle is applied to generate the MRELBP histogram feature, while considering the fusion of the three feature sets related to the central density (CI), the neighborhood density (NI) and the radial difference (RD) expressed in (Eq.6), (Eq.7) and (Eq.8).

In summary, the global grayscale variation rule may be reliably understood by the MRELBP-CI augmented through the medium filter. As for MRELBP-NI, the center pixel and its neighbors are both replaced by medium-filtered grayscale values within a few patches, which can achieve zero-mean of the local neighborhood and eventually has superior anti-noise and anti-illumination-change. The MRELBP-RD will collect

the edge-like information lost by the previous two intensity-based sub-descriptors. Therefore, the concatenated histograms in Figure 2 are considered sufficient for image classification because they are informative, noise-resistant, and scale-invariant.

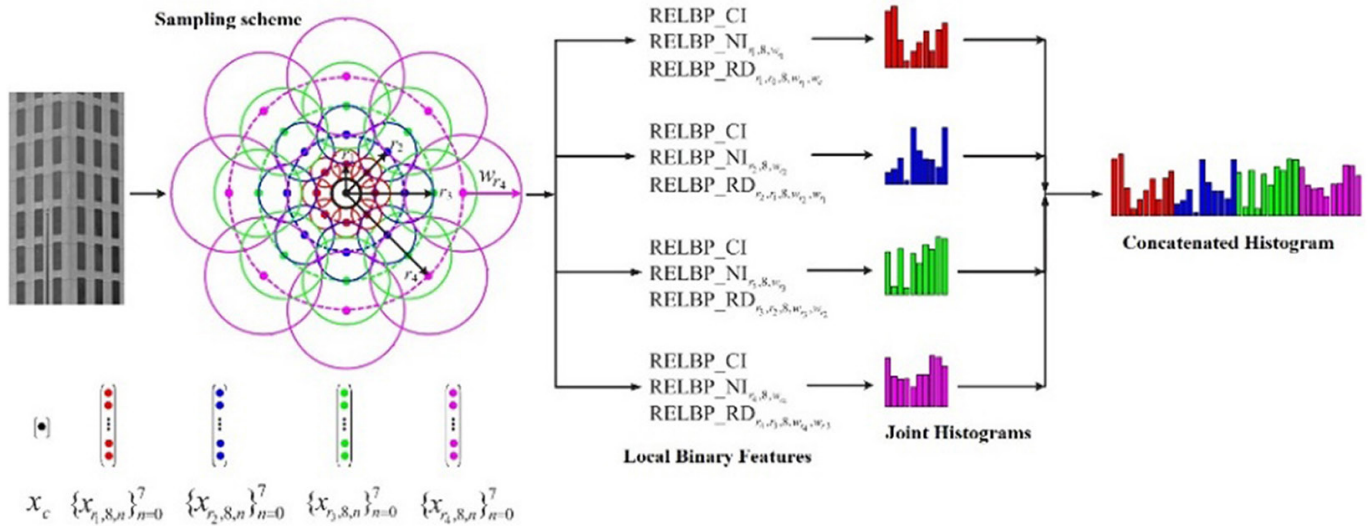


Fig. 2. MRELBP features histograms extraction scheme extracted from [16]

Classification. In this section, we present a brief overview of the classification phase algorithms. Mainly, SVMs, MLP, KNN, and RF.

SVMs classifier: SVM is a powerful supervised learning method initially proposed by Vapnik [46]. It consists of a set of training instances to determine optimal hyperplanes that have the maximum margin. Many SVM [47] varieties are proposed to solve the non-linear and multi-class classification problems. For a non-linear problem, we use polynomial or RBF kernels, while the multi-class problem is decomposed into several binary problems using one-against-all or one against-one strategy.

- Polynomial kernel is expressed as:

$$K(x, y) = (\langle x, y \rangle)^d. \text{ Where, } d = 1, 2, 3, \dots \quad (9)$$

- RBF kernel is expressed as:

$$K(x, y) = \exp\left(-\frac{\|x - y\|^2}{2\sigma^2}\right). \text{ Where, } \sigma \text{ is the variance} \quad (10)$$

RF classifier: RF [48] is a supervised machine learning algorithm that consists of multiple decision trees learning. To establish its final outcome, RF combines predictions of its decision trees through bagging or bootstrap aggregating algorithms. The main steps of RF are:

- Step-1:** Select random data samples from the training set.
- Step-2:** Generate a decision tree for selected data samples (Subsets).
- Step-3:** Select the number of the decision trees you want to create.
- Step-4:** Repeat Step 1 and 2.
- Step-5:** For new data samples, find the predictions of each decision tree and assign the new data samples to the category that wins the majority votes.

In our case, we use a forest of 50 trees, 170 nodes for each tree.

MLP classifier: MLP [49] is one of the most widely used neural networks in machine learning. It consists of input, output and hidden layers. Moreover, MLP adjusts the weights of its neurons using supervised procedures, primarily, back-propagation that learns the network through three phases: forward propagation, backward propagation and weight adaptation. The optimal MLP model is generally determined by the number of hidden layers and the number of neurons in each hidden layer. In our case, we use two hidden layers of 48 and 32 neurons, respectively.

KNN classifier: One of the simplest supervised learning algorithms is the KNN classifier [50]. It consists of classifying each new sample of the training set using the k nearest neighbors, which are determined using several similarity measures, particularly Euclidean norms; in this case, $k = 2$, with Manhattan distance.

4 EXPERIMENTAL

This section presents the experimental results of the proposed approach and its comparison with the state-of-the-art along with a discussion.

4.1 Dataset

In this study, the various evaluation tests are performed on the Kvasir-Capsule dataset [51], readily available from the Open Science Framework (OSF). This dataset consists of 118 videos captured using the Olympus EC-S10 endo-capsule. An overview of this dataset is summarized in Table 1, which includes a total of 4,820,857 primary data records. Among these records, there are 44,228 labeled images with bounding box masks, 44 corresponding labeled videos, and 74 unlabeled videos.

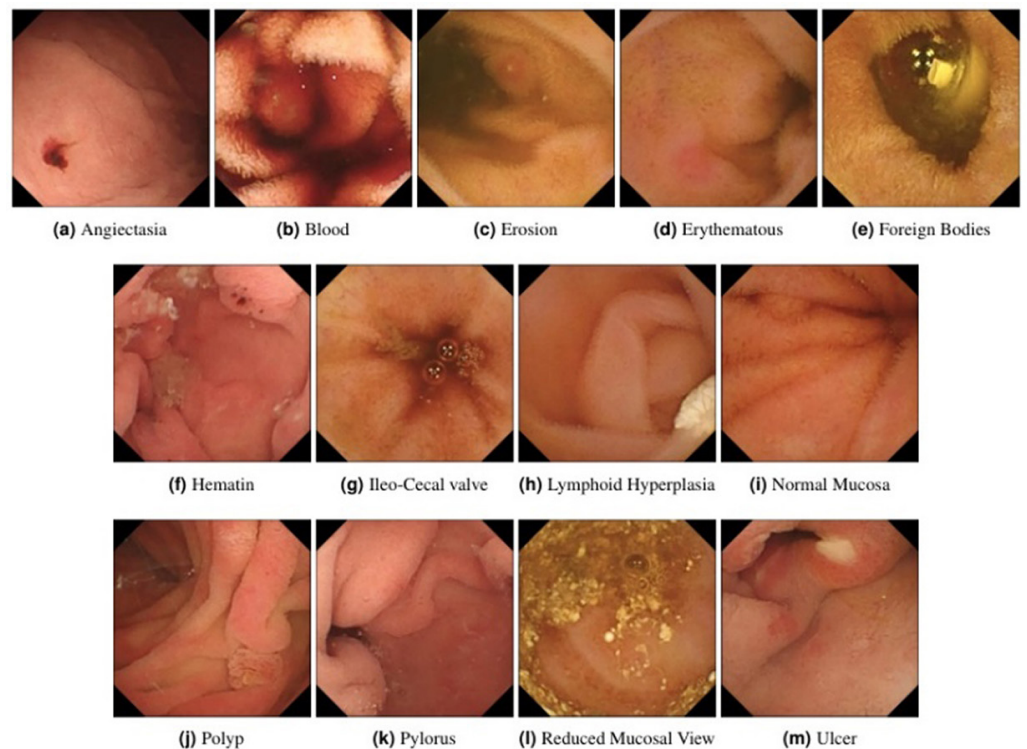
Since our aim is to distinguish between normal images and ulcerous ones, we focus on the 44,228 labeled images stored in the PNG format. Table 2 illustrates the distribution of these labeled images across 13 different classes, each representing a specific category of findings, along with the corresponding number of images in each class. See Figure 3. As we can see, the number of images per class is imbalanced, which is a common challenge in medical datasets. This class imbalance can impact the performance of data-driven algorithms, particularly when certain findings occur more frequently than others. In our case, to address the imbalance issue, we exclusively selected 1000 images from the normal dataset to have a representative sample of normal cases. By doing so, we avoided the problem of an imbalanced dataset and focused on a specific pathology of interest. Additionally, we also included whole ulcer images from the ulcer folder, which consists of 854 images, to have a representative sample of ulcer cases.

Table 1. Overview of the Kvasir-Capsule dataset

Types	Labeled	Unlabeled
Images	44,228	4,776,479
Videos	44	74

Table 2. Number of labeled images per each class

Class Label	Class Name	Number of Images
a	Angiectasia	866
b	Blood	446
c	Erosion	438
d	Erythematous	238
e	Foreign Bodies	776
f	Hematin	12
g	Ileo-Cecal valve	1,417
h	Lymphoid Hyperplasia	592
i	Normal Mucosa	34,606
j	Polyp	64
k	Pylorus	1,520
l	Reduced Mucosal View	2,399
m	Ulcer	854

**Fig. 3.** One image per class of Kvasir-Capsule dataset

4.2 Evaluation protocol

In order to conduct a comprehensive evaluation of our approach, we proposed the following evaluation protocol:

- Decompose the original WCE images dataset into six image datasets following each of the six color components (R/G/B/Y/Cb/Cr).
- For each color component:
 - Build the selected features-set by applying descriptors on the image dataset.
- For each classifier:
 - Configure settings, use the cross-validation method with 5-fold and take 80% of dataset as training set and remaining 20% as testing set.
 - Generate the confusion matrix and record the accuracy value.
 - Compare results with other works.

To evaluate classifier performance, a confusion matrix must be generated. This helps determine metrics as F-measure, recall, precision, and accuracy. In our case, the dataset is almost balanced, which favored the adoption of accuracy as an evaluation criterion.

4.3 Results and Discussion

Based on the previous evaluation protocol, we carried out three experiments by using the reduced Kvasir-Capsule dataset.

Experiment-1: In this experiment, we applied the previously provided classifiers to classify different sets of selected $MRELBP^{riu2}$ features in relation to each color component. The results obtained through the confusion matrices (See Figure 4) are accessible in Table 3 below. From these results, we can conclude that the RBF variant of the SVM classifier performed exceptionally well, achieving an impressive accuracy of 97.04% on the B color channel. Furthermore, the RF classifier also demonstrated strong performance, achieving an accuracy of 96.77% on the color R channel. Also, it can note that the (RF) classifier has demonstrated its performance by achieving an accuracy of 96.77% on the color R channel. Additionally, other classifiers exhibited outstanding performances according to specific color channels. For instance, on the R channel, the KNN, SVM (Poly-3, $d = 3$), and SVM (RBF) achieved high accuracies of 95.14%, 95.15%, and 95.69%, respectively. Similarly, on the G channel, KNN, SVM (Linear), and SVM (Poly-2, $d = 2$) reached accuracies of 95.14%, 93.26%, and 95.15%, respectively. On the B channel, KNN, SVM (Poly-1, $d = 1$), and SVM (Poly-3) achieved accuracies of 96.49%, 93.26%, and 94.34%, respectively. Furthermore, these classifiers also demonstrated strong performance in the YCbCr color space. Specifically, on the Y channel, the KNN achieved an accuracy of 96.22%, while SVM (RBF) and RF achieved accuracies of 95.96% and 95.69, respectively. On the Cb channel, both KNN, and SVM (Poly-2) reached an accuracy of 93.53%. Finally, on the Cr channel., SVM (RBF) and RF achieved accuracies of 92.99% and 92.18%, respectively. In order to properly assess the performance of the proposed approach, we suggest two experiments. In the first, we redeployed the dataset from Saoudi's [38] work. In the second, we tested the same dataset using the most popular pre-trained CNNs.

	Normal	Ulcer		Normal	Ulcer		Normal	Ulcer		Normal	Ulcer
Normal	958	42	Normal	956	44	Normal	952	48	Normal	961	39
Ulcer	18	836	Ulcer	21	833	Ulcer	26	828	Ulcer	16	838
	(a) RF-R			(b) KNN-B			(c) RBF-Y			(d) RBF-B	

Fig. 4. Confusion matrices of the four best results

Table 3. Results of different classifiers on $MRELBP_{1,8}^{riu2}$

Color		R	G	B	Y	Cb	Cr
RF		96.77(a)	94.34	93.53	95.69	90.84	92.18
KNN		95.14	95.14	96.49(b)	96.22	93.53	85.17
MLP		88.21	89.19	87.84	89.49	90.30	88.68
SVMs	Linear	91.37	93.26	90.03	92.72	85.98	88.68
	Poly-1	91.37	90.57	93.26	91.91	90.30	88.68
	Poly-2	95.15	95.15	94.61	93.53	93.53	89.49
	Poly-3	90.57	92.45	94.34	90.57	81.94	82.48
	RBF	95.69	95.69	97.04(d)	95.96(c)	92.45	92.99

Notes: The (a), (b), (c) and (d) are refer to the confusion matrix from Figure 4. The bold numbers are refer to the maximum values.

Experiment-2: In this experiment, we applied the conditions of experiment-1 to classify different sets of selected $MsCLBP$ features according to each color component. The results of $MsCLBP_M$ and $MsCLBP_S$ are accessible in Tables 4 and 5, respectively. From these results, Tables 4 and 5, it is clear that the accuracies of KNN, MLP, SVM(Linear), SVM(Poly-1), and SVM(Poly-3) are relatively low when compared to RF and SVM(Poly-2). For example, RF achieved an accuracy of 92.70% with $MsCLBP_S$ on the color Cr channel. Similarly, SVM(Poly-2) achieved an accuracy of 95.15% with $MsCLBP_M$ for the color R and G channels. Comparing the results from Tables 3, 4, and 5, it is evident that $MRELBP$'s performance significantly outperforms $MsCLBP$'s for nearly all components and color classifiers. To further underscore the effectiveness of our approach, we will compare it with recent deep learning-based methods. This is the primary focus of experiment-3.

Table 4. Results of different classifiers on $MsCLBP_M_{1,8}^{riu2}$

Color		R	G	B	Y	Cb	Cr
RF		86.76	86.76	85.68	87.03	86.22	85.68
KNN		85.17	81.67	82.74	84.63	86.79	86.79
MLP		81.08	76.22	79.46	76.49	82.43	82.70
SVMs	Linear	76.55	69.27	73.85	72.78	80.86	66.85
	Poly-1	80.81	72.70	79.19	74.60	81.35	76.22
	Poly-2	95.15	95.15	94.61	93.53	93.53	89.49
	Poly-3	81.94	72.24	79.51	74.66	79.25	80.59
	RBF	79.25	76.28	72.51	80.05	77.63	73.32

Note: The bold number is refer to the maximum value.

Table 5. Results of different classifiers on $MsCLBP_S_{1,8}^{riu2}$

Color		R	G	B	Y	Cb	Cr
RF		84.87	84.60	85.95	86.76	90.27	92.70
KNN		79.78	79.51	81.40	80.32	86.52	86.52
MLP		81.62	74.32	83.24	78.92	79.73	84.87

(Continued)

Table 5. Results of different classifiers on MsCLBP_S_{1,8}^{riu2} (Continued)

Color		R	G	B	Y	Cb	Cr
SVMs	Linear	69.81	67.39	73.85	68.73	68.19	74.66
	Poly-1	77.03	73.24	74.32	72.70	76.76	82.70
	Poly-2	82.48	70.08	77.09	73.32	82.75	80.59
	Poly-3	78.71	76.55	77.63	77.63	83.02	78.71
	RBF	85.98	82.21	84.64	82.48	88.95	85.98

Note: The bold number is refer to the maximum value.

Experiment-3: In this experiment, our main objective is to compare our proposed approach with the most relevant and recent, deep learning-based methods found in the literature. To achieve this, we applied four benchmark pre-trained CNN models, namely Alexnet [26], MobileNetv2 [32], Resnet18, and Resnet50 [52], to the original RGB image dataset as described in Experiment-1. The results obtained are shown in Table 6. It is important to note that for our proposed approach, we reported the top three accuracy scores along with their corresponding classifiers and color channels. From these results, it is evident that our proposed approach consistently outperforms the Resnet 50 architecture, regardless of the classifier or color channel used. The Mobilnetv2 architecture slightly outperforms our approach, but only when using the KNN classifier. The Resnet 18 achieves the same accuracy as the SVM classifier with the RBF kernel on channel B. The only notable exception is the Alexnet architecture, which slightly outperforms all classifiers used in our approach.

Table 6. Accuracy comparison between MRELBP and others deep-learning methods

Method	Color	Classifier	Accuracy
Our approach	R	RF	96.77
	B	RBF	97.04
	B	KNN	96.49
Resnet18 [52]	RGB		97.04
Resnet50 [52]	RGB		94.07
Alexnet [26]	RGB		97.57
Mobilenetv2 [32]	RGB		96.71

In conclusion, a comparison of our approach with previous pre-trained CNNs shows that our approach remains competitive with an accuracy of 97,04% against 97.57% for the Alexnet, knowing that pre-trained CNNs usually require deep learning algorithms which are more computationally expensive than machine learning algorithms. Moreover, we must notice that in our case, results for only one-color component are considered. However, for the deep learning-based competitors' approaches, all color components were involved. This means more time computing and more relevant information that we were deprived of. distance.

5 CONCLUSION

In this paper, we proposed a robust approach to classify ulcer/non-ulcer images from WCE examination. It is based on the medial robust local binary pattern (MRLBP), which has shown its superiority in previous works, to solve problems

related to the acquisition conditions, namely illumination, contrast, rotation and noise. After a pre-processing step using the Power Law Transformation (PLT) algorithm to enhance the contrast of RGB and YCbCr images, the MRLBP is computed for each resulting color component to extract texture color features. The effectiveness of the proposed approach is largely validated by the experimental results that have been carried out using the Kvasir-Capsule dataset. Thus, our approach outperformed methods based on the fusion of LBP-like descriptors and machine learning algorithms. Besides, it remains very competitive with methods based on deep learning algorithms by achieving an accuracy of 97.04% versus 97.57% for the Alexnet. However, there is a dependency between color components that has been partially ignored in our case. As future work, we plan to exploit these dependencies and include other datasets to improve the performance of the computer-aided diagnostic systems playing a critical role in medical images interpretation.

6 REFERENCES

- [1] A. Bourouhou, A. Jilbab, C. Nacir, and A. Hammouch, "Heart sound signals segmentation and multiclass classification," *International Journal of Online & Biomedical Engineering*, vol. 16, no. 15, pp. 64–79, 2020. <https://doi.org/10.3991/ijoe.v16i15.16817>
- [2] S. A. Alomari, "An efficient system for diagnosis of human blindness using image-processing and machine-learning methods," *International Journal of Online & Biomedical Engineering*, vol. 19, no. 10, pp. 82–98, 2023. <https://doi.org/10.3991/ijoe.v19i10.37681>
- [3] A. Ouhmida, A. Raihani, B. Cherradi, and O. Terrada, "A novel approach for Parkinson's disease detection based on voice classification and features selection techniques," *International Journal of Online & Biomedical Engineering*, vol. 17, no. 10, pp. 111–130, 2021. <https://doi.org/10.3991/ijoe.v17i10.24499>
- [4] B. Jabłońska and S. Mrowiec, "Gastrointestinal disease: New diagnostic and therapeutic approaches," *Biomedicines*, vol. 11, no. 5, p. 1420, 2023. <https://doi.org/10.3390/biomedicines11051420>
- [5] A. Tollivoro *et al.*, "Index colonoscopy-related risk factors for postcolonoscopy colorectal cancers," *Gastrointestinal Endoscopy*, vol. 89, no. 1, pp. 168–176, 2019. <https://doi.org/10.1016/j.gie.2018.08.023>
- [6] W. Marlicz *et al.*, "Frontiers of robotic gastroscopy: A comprehensive review of robotic gastroscopes and technologies," *Cancers*, vol. 12, no. 10, p. 2775, 2020. <https://doi.org/10.3390/cancers12102775>
- [7] Y. Horiuchi, K. Aoyama, Y. Tokai *et al.*, "Convolutional neural network for differentiating gastric cancer from gastritis using magnified endoscopy with narrow band imaging," *Digestive Diseases and Sciences*, vol. 65, pp. 1355–1363, 2020. <https://doi.org/10.1007/s10620-019-05862-6>
- [8] K. Timothy and C. Brooks, "Principles of gastrointestinal endoscopy," *Surgery (Oxford)*, vol. 41, no. 2, pp. 100–105, 2023. <https://doi.org/10.1016/j.mpsur.2022.11.005>
- [9] G. Iddan, G. Meron, A. Glukhovsky *et al.*, "Wireless capsule endoscopy," *Nature*, vol. 405, no. 6785, pp. 417–417, 2000. <https://doi.org/10.1038/35013140>
- [10] T. Rahim, M. A. Usman, and S. Y. Shin, "A survey on contemporary computer-aided tumor, polyp, and ulcer detection methods in wireless capsule endoscopy imaging," *Computerized Medical Imaging and Graphics*, vol. 85, p. 101767, 2020. <https://doi.org/10.1016/j.compmedimag.2020.101767>
- [11] M. Hajabdollahi, R. Esfandiarpour, E. Sabeti, N. Karimi, S. M. R. Soroushmehr, and S. Samavi, "Multiple abnormality detection for automatic medical image diagnosis using bifurcated convolutional neural network," *Biomedical Signal Processing and Control*, vol. 57, p. 101792, 2020. <https://doi.org/10.1016/j.bspc.2019.101792>

- [12] T. Tamaki *et al.*, “Computer-aided colorectal tumor classification in NBI endoscopy using local features,” *Medical Image Analysis*, vol. 17, no. 1, pp. 78–100, 2013. <https://doi.org/10.1016/j.media.2012.08.003>
- [13] M. Souaidi, A. A. Abdelouahad, and M. E. Ansari, “A fully automated ulcer detection system for wireless capsule endoscopy images,” in *Proc. International Conference on Advanced Technologies for Signal and Image Processing (ATSIP)*, 2017, pp. 1–6. <https://doi.org/10.1109/ATSIP.2017.8075599>
- [14] Y. Wang, W. Tavanapong, J. Wong, J. Oh, and P. C. de Groen, “Part-based multiderivative edge cross-sectional profiles for polyp detection in colonoscopy,” *IEEE Journal of Biomedical and Health Informatics*, vol. 18, no. 4, pp. 1379–1389, 2014. <https://doi.org/10.1109/JBHI.2013.2285230>
- [15] F. Rusta *et al.*, “Wireless capsule endoscopy bleeding images classification using CNN based model,” *IEEE Access*, vol. 9, pp. 33675–33688, 2021. <https://doi.org/10.1109/ACCESS.2021.3061592>
- [16] L. Liu, S. Lao, P. W. Fieguth, Y. Guo, X. Wang, and M. Pietikäinen, “Median robust extended local binary pattern for texture classification,” *IEEE Transactions on Image Processing*, vol. 25, no. 3, pp. 1368–1381, 2016. <https://doi.org/10.1109/TIP.2016.2522378>
- [17] T. Ahonen, A. Hadid, and M. Pietikainen, “Face description with local binary patterns: Application to face recognition,” *IEEE Transactions on Pattern Analysis and Machine Intelligence*, vol. 28, no. 12, pp. 2037–2041, 2006. <https://doi.org/10.1109/TPAMI.2006.244>
- [18] H. Finsterer, “Malignant degeneration of gastric ulcerer: (Section of Surgery),” in *Proc. of the Royal Society of Medicine*, vol. 32, no. 3, pp. 183–196, 1939. <https://doi.org/10.1177/003591573903200315>
- [19] L.-E. Hansson, O. Nyrén, A. W. Hsing, R. Bergström, S. Josefsson, W.-H. Chow, J. F. Fraumeni, and H.-O. Adami, “The risk of stomach cancer in patients with gastric or duodenal ulcer disease,” *New England Journal of Medicine*, vol. 335, no. 4, pp. 242–249, 1996. <https://www.nejm.org/doi/full/10.1056/nejm199607253350404>
- [20] L. R. Al-Khazraji, A. R. Abbas, and A. S. Jamil, “The effect of changing targeted layers of the deep dream technique using VGG-16 model,” *International Journal of Online & Biomedical Engineering*, vol. 19, no. 3, pp. 34–47, 2023. <https://doi.org/10.3991/ijoe.v19i03.37235>
- [21] L. R. Al-Khazraji, A. R. Abbas, and A. S. Jamil, “A systematic review of deep dream,” *IRAQI J. Comput. Commun. Control Syst. Eng.*, vol. 23, pp. 192–209, 2023. <https://doi.org/10.33103/uot.ijccce.23.2.15>
- [22] D. K. Iakovidis, S. V. Georgakopoulos, M. Vasilakakis, A. Koulaouzidis, and V. P. Plagianakos, “Detecting and locating gastrointestinal anomalies using deep learning and iterative cluster unification,” *IEEE Transactions on Medical Imaging*, vol. 37, no. 10, pp. 2196–2210, 2018. <https://doi.org/10.1109/TMI.2018.2837002>
- [23] T. Aoki *et al.*, “Automatic detection of erosions and ulcerations in wireless capsule endoscopy images based on a deep convolutional neural network,” *Gastrointestinal Endoscopy*, vol. 89, no. 2, pp. 357–363, 2019. <https://doi.org/10.1016/j.gie.2018.10.027>
- [24] W. Liu, *et al.*, “SSD: Single shot multibox detector,” In *Computer Vision – ECCV 2016, ECCV 2016*, Leibe, B., Matas, J., Sebe, N., and Welling, M. Eds., Lecture Notes in Computer Science, Springer, 2016, vol. 9905. https://doi.org/10.1007/978-3-319-46448-0_2
- [25] S. Wang, Y. Xing, L. Zhang, H. Gao, and H. Zhang, “Deep convolutional neural network for ulcer recognition in wireless capsule endoscopy: Experimental feasibility and optimization,” *Computational and Mathematical Methods in Medicine*, vol. 2019, 2019. <https://doi.org/10.1155/2019/7546215>
- [26] H. Alaskar, A. Hussain, N. Al-Aseem, P. Liatsis, and D. Al-Jumeily, “Application of convolutional neural networks for automated ulcer detection in wireless capsule endoscopy images,” *Sensors*, vol. 19, no. 6, p. 1265, 2019. <https://doi.org/10.3390/s19061265>
- [27] Y. Yuan and M. Meng, “Deep learning for polyp recognition in wireless capsule endoscopy images,” *Medical Physics*, vol. 44, no. 4, pp. 1379–1389, 2017. <https://doi.org/10.1002/mp.12147>

- [28] A. Krizhevsky, I. Sutskever, and G. Hinton, "Image net classification with deep convolutional neural networks," in *Proc. of the Advances in Neural Information Processing Systems*, Lake Tahoe, NV, USA, 2012, pp. 1097–1105.
- [29] V. Vani and K. V. Mahendra Prashanth, "Ulcer detection in wireless capsule endoscopy images using deep CNN," *Journal of King Saud University – Computer and Information Sciences*, vol. 34, no. 6, pp. 3319–3331, 2022. <https://doi.org/10.1016/j.jksuci.2020.09.008>
- [30] A. Rehman, "Ulcer recognition based on 6-layers deep convolutional neural network," in *Proc. of the 9th International Conference on Software and Information Engineering*, 2020, pp. 97–101. <https://doi.org/10.1145/3436829.3436837>
- [31] A. Ellahyani, I. El jaafari, and S. Charfi, "Computer-aided diagnosis system for ulcer detection in wireless capsule endoscopy images," *Journal of Physics: Conference Series*, vol. 1743, *The International Conference on Mathematics & Data Science (ICMDS)*, 2020 Khouribga, Morocco. <https://doi.org/10.1088/1742-6596/1743/1/012016>
- [32] M. Alhajlah, "Robust ulcer classification: Contrast and illumination invariant approach," *Diagnostics*, vol. 12, p. 2898, 2022. <https://doi.org/10.3390/diagnostics12122898>
- [33] B. Li and M. Q.-H. Meng, "Texture analysis for ulcer detection in capsule endoscopy images," *Image and Vision Computing*, vol. 27, no. 9, pp. 1336–1342, 2009. <https://doi.org/10.1016/j.imavis.2008.12.003>
- [34] V. Charisis, A. Tsiligiri, L. J. Hadjileontiadis, C. N. Liatsos, C. C. Mavrogiannis, and G. D. Sergiadis, "Ulcer detection in wireless capsule endoscopy images using bidimensional nonlinear analysis," in *Proc. of the XII Mediterranean Conference on Medical and Biological Engineering and Computing*, 2010, vol. 29. https://doi.org/10.1007/978-3-642-13039-7_59
- [35] L. Yu, P. C. Yuen, and J. Lai, "Ulcer detection in wireless capsule endoscopy images," in *Proc. of the 21st International Conference on Pattern Recognitio*, Tsukuba, Japan, 2012, pp. 45–48.
- [36] J. Yeh, T. Wu, and W. Tsai, "Bleeding and ulcer detection using wireless capsule endoscopy images," *Journal of Software Engineering and Applications*, vol. 7, pp. 422–432, 2014. <https://doi.org/10.4236/jsea.2014.75039>
- [37] S. Charfi, M. El Ansari, and I. Balasingham, "Computer-aided diagnosis system for ulcer detection in wireless capsule endoscopy images," *IET Image Processing*, vol. 13, no. 6, pp. 1023–1030, 2019. <https://doi.org/10.1049/iet-ipr.2018.6232>
- [38] M. Souaidi, A. Ait Abdelouahed, and M. El Ansari, "Multi-scale completed local binary patterns for ulcer detection in wireless capsule endoscopy images," *Multimedia Tools and Applications*, vol. 78, pp. 13091–13108, 2019. <https://doi.org/10.1007/s11042-018-6086-2>
- [39] R. Ponnusamy, S. Sathiamoorthy, and R. Visalaksh, "An efficient method to classify GI tract images from WCE using visual words," *International Journal of Electrical and Computer Engineering (IJECE)*, vol. 10, no. 6, pp. 5678–5686, 2020. <https://doi.org/10.11591/ijece.v10i6.pp5678-5686>
- [40] J. Naz, M. Sharif *et al.*, "Recognizing gastrointestinal malignancies on WCE and CCE images by an ensemble of deep and handcrafted features with entropy and PCA based features optimization," *Neural Processing Letters*, vol. 55, no. 1, pp. 115–140, 2023. <https://doi.org/10.1007/s11063-021-10481-2>
- [41] C. M. Tsai, "Adaptive local power-law transformation for color image enhancement," *Applied Mathematics & Information Sciences*, vol. 7, no. 5, pp. 2019–2026, 2013. <https://doi.org/10.12785/amis/070542>
- [42] T. Ojala and M. Pietikäinen, "Unsupervised texture segmentation using feature distributions," *Pattern Recognition*, vol. 32, no. 3, pp. 477–486, 1999. [https://doi.org/10.1016/S0031-3203\(98\)00038-7](https://doi.org/10.1016/S0031-3203(98)00038-7)
- [43] R. Davarzani, S. Mozaffari, and K. Yaghmaie, "Scale-and rotation-invariant texture description with improved local binary pattern features," *Signal Processing*, vol. 111, pp. 274–293, 2015. <https://doi.org/10.1016/j.sigpro.2014.11.005>

- [44] Z. Guo and L. Zhang, "A completed modeling of local binary pattern operator for texture classification," *IEEE Transactions on Image Processing*, vol. 19, no. 6, pp. 1657–1663, 2010. <https://doi.org/10.1109/TIP.2010.2044957>
- [45] L. Li, L. Zhao, Y. Long, G. Kuang, and P. Fieguth, "Extended local binary patterns for texture classification," *Image and Vision Computing*, vol. 30, no. 2, pp. 86–99, 2012. <https://doi.org/10.1016/j.imavis.2012.01.001>
- [46] C. Cortes and V. Vapnik, "Support-vector networks," *Machine Learning*, vol. 20, pp. 273–297, 1995. <https://doi.org/10.1007/BF00994018>
- [47] C. Chang and C.-J. Lin, "LIBSVM: A library for support vector machines," *ACM Transactions on Intelligent Systems and Technology*, vol. 2, no. 3, pp. 1–27, 2011. <https://doi.org/10.1145/1961189.1961199>
- [48] M. Pal, "Random forest classifier for remote sensing classification," *International Journal of Remote Sensing*, vol. 26, no. 1, pp. 217–222, 2005. <https://doi.org/10.1080/01431160412331269698>
- [49] S. Osowski, K. Siwek, and T. Markiewicz, "MLP and SVM networks-a comparative study," in *Proc. of the 6th Nordic Signal Processing Symposium*, 2004. NORSIG 2004, Espoo, Finland, 2004, pp. 37–40.
- [50] S. Zhang, X. Li, M. Zong, X. Zhu, and D. Cheng, "Learning k for knn classification," *ACM Transactions on Intelligent Systems and Technology*, vol. 8, no. 3, pp. 1–19, 2017. <https://doi.org/10.1145/2990508>
- [51] P. H. Smedsrud *et al.*, "Kvasir-Capsule, a video capsule endoscopy dataset," *Scientific Data*, vol. 8, p. 142, 2021. <https://doi.org/10.1038/s41597-021-00920-z>
- [52] K. He, X. Zhang, S. Ren, and J. Sun, "Deep residual learning for image recognition," in *Proc. of IEEE Conference on Computer Vision and Pattern Recognition (CVPR)*, 2016, pp. 770–778. <https://doi.org/10.1109/CVPR.2016.90>

7 AUTHORS

Abdellatif Dahmouni received a PhD degree from the USMBA University in 2019. He is currently a professor of computer science at the UCD University in Morocco. His research interests include Artificial Intelligence and pattern recognition (E-mail: dahmouni.a@ucd.ac.ma).

Abdelkader Ait Abdelouahad received his Ph.D. degree from the Mohammed V University in 2013. He is currently an associate professor of computer science at the UCD University in Morocco. His research interests include Artificial Intelligence, Computer Vision and Multimedia (AIM).

Yasser Aderghal received his MSc degree in Business Intelligence & Big Data Analytics from UCD University in 2023. Now, he is a PhD student in deep learning and natural language processing at the IUR University of Rabat in Morocco.

Ibrahim Guelzim received the PhD degree from the Mohammed V University in 2012. He is currently an associate professor of computer science at the Hassane 2 University in Morocco. His research interests include Artificial Intelligence, Computer Vision and Image Processing.

Insaf Bellamine received his PhD degree from the USMBA University in 2017. He is currently an associate professor of computer science at the UCD University in Morocco. His research interests include Artificial Intelligence, Computer Vision and Image and Video Processing.

Hassan Silkan received his PhD degree from the USMBA University in 2009. He is currently a full professor of computer science at the UCD University in Morocco. His research interests include Artificial Intelligence, Computer Vision and Image Processing.